CrossMark
click for updates

provided by low cost, natural abundance of the components, relatively good refractoriness, high electrical conductivity and compatibility with molten silicates. Their chemical composition represents another advantage, since partial dissolution will not contaminate the electrolyte and may even account for a fraction of raw iron oxide source. Previous works have demonstrated how the redox stability and high-temperature electrical properties can be tuned by various substitutions in Fe_3O_4, including magnesium, aluminum and some transition metal cations.[9,12 14] In particular, the substitution with magnesium is advantageous for the refractoriness, while the redox stability and charge transport are strongly linked to the oxidation states of the substituting cations.[9,14]

The approach to design the spinel composition through various simultaneous co-substitutions may have a great potential for many applications, by introducing complex magnetic interactions, specific changes in electronic band structure and redox states/coordination of the constituent cations, promoted by various mutual effects. This methodology was implemented for several low-temperature applications, including magnetic nanoparticles,[15,16] catalysts[17] and cathode materials for lithium rechargeable batteries (*e.g.*,[18]). In the present work, this approach was assessed assuming the high-temperature applications of the ferrospinels, containing various cations, in the form of bulk materials, eventually targeting the development of suitable anodes for pyroelectrolysis. Multicomponent ferrospinel-based consumable anodes may be suitable for simultaneous co-electroreduction of transition metal cations with iron to produce alloys. Although this concept is still far from convincing, even at lab-scale, recent results on demonstration of the pyroelectrolysis process[19] are enough promising to consider it as potentially attractive. Thus, this work was focused on the relevant structural, thermal, transport and redox properties of the magnetite-based multicomponent spinels. The presence of magnesium in the composition is favourable for improving refractoriness and redox stability of these materials.[9] Therefore, the selected composition range is derived from $Fe_{2.8}Mg_{0.2}O_4$ with simultaneously co-additions of transition metal cations with different redox behaviour, namely Cr, Ti, Mn, Ni. These additives are also relevant for alloying in steel production, envisaging the pyroelectrolysis concept.

2. Experimental

The chemical composition of the ferrospinels was selected based on the Taguchi method,[20] in order to optimize the experimental plan and minimize the number of compositions required to assess the role of different transition metal cations. In general, the studied materials can be represented as $Fe_{2.8-x-y-z-p}Mg_{0.2}Cr_xTi_yMn_zNi_pO_4$ (CTMN), where $x+y+z+p \leq 0.5$. The list of the compositions and their denominations are given in Table 1.

The precursor powders of CTMN spinels were prepared by mixing the stoichiometric amounts of $FeC_2O_4 \cdot 2H_2O$ (99%, Sigma-Aldrich), $Mg(NO_3)_2 \cdot 6H_2O$ (99%, Avocado Research Chemicals), $Cr(NO_3)_3 \cdot 9H_2O$ (99%, Sigma-Aldrich), TiO_2 (99.8%, Sigma-Aldrich), $Mn(CH_3COO)_2 \cdot 4H_2O$ (≥99%, Aldrich) and $Ni(NO_3)_2 \cdot 6H_2O$ (≥98.5%, Sigma-Aldrich), followed by several calcinations at 1173–1373 K with multiple intermediate grindings. Assuming homogeneous distribution of the cations, the maximum deviation from the stoichiometry set by the ratio of the precursors was fairly below ±0.001. Corresponding "as-prepared" ceramic samples were sintered at 1773 K for 10 h in Ar atmosphere ($p(O_2) \sim 10^{-5}$ to 10^{-4} atm). These samples were used for SEM/EDS, electrical conductivity and thermal expansion measurements, while X-ray diffraction (XRD) and thermogravimetry (TG) were performed on the powders, prepared by grinding corresponding ceramics in a mortar. The experimental density of the ceramics was assesses by the Archimedes method.

The room-temperature XRD patterns were recorded using a Rigaku D/Max-B diffractometer (CuK_α, 2Θ = 10–80°, step 0.02°, exposition 2 s) and were used for the determination of the phase composition and calculation of the unit cell parameters by the profile matching method in Fullprof software.[21] The phase content was also quantified by Rietveld analysis, using Jade 9 (PDF-2) software. Additional assessment of the phase purity, homogeneity and microstructural features was performed by complementary SEM (Hitachi SU-70 instrument) and EDS (Bruker Quantax 400 detector) studies on fractured ceramics. Redox behaviour of the powdered as-prepared samples was studied by thermogravimetry (TG) (Setaram Set-Sys 16/18 instrument, sensitivity 0.4 μg, initial sample weight ~0.5 g), in a flow of argon or dry air at 298–1373 K with constant

Table 1 Compositions of $Fe_{2.8-x-y-z-p}Cr_xTi_yMn_zNi_pMg_{0.2}O_4$ CTMN spinels, lattice parameter (*a*) and electrical conductivity at 1623 K (σ_{1623})

x	*y*	*z*	*p*	Notation	*a* (nm)	ρ_{exp}/ρ_{theor} (%)	σ_{1623}, (S cm ^{1})
0	0	0	0	C0T0M0N0	0.83918(3)	80	104
0.05	0.05	0.05	0.05	C5T5M5N5	0.83987(3)	81	89
0.05	0.15	0.1	0.1	C5T15M10N10	0.84092(3)	78	65
0.05	0.1	0.15	0.15	C5T10M15N15	0.84104(3)	81	47
0.1	0.05	0.1	0.15	C10T5M10N15	0.83919(3)	78	59
0.1	0.1	0.05	0.05	C10T10M5N10	0.83975(3)	77	70
0.1	0.15	0.15	0.05	C10T15M15N5	0.84010(3)	77	50
0.15	0.05	0.15	0.1	C15T5M15N10	0.84197(4)	82	50
0.15	0.1	0.1	0.05	C15T10M10N5	0.84059(2)	79	53
0.15	0.15	0.05	0.15	C15T15M5N15	0.84008(3)	83	62

heating/cooling rate of 2 K min^{-1}. Thermal expansion studies were performed on heating (3 K min^{-1}) in argon and air atmospheres up to 1350 K, using a vertical alumina dilatometer Linseis L70/2001. Total electrical conductivity (σ) was measured by 4-probe DC technique at 1075–1773 K in the oxygen partial pressure $p(O_2)$ range from 10^{-5} to 0.21 atm in flowing air–Ar mixtures. The $p(O_2)$ in the gas flow was monitored using an electrochemical yttria-stabilized zirconia (YSZ)-based oxygen sensor. For two compositions the preparation procedure was repeated under the same conditions in order to check the reproducibility of the electrical properties. Corresponding variations in the electrical conductivities between the samples of the same nominal composition from different batches was below 5%.

3. Results and discussion

The results of XRD analysis, performed for the as-prepared samples, indicate that all studied compositions are single-phase spinels (space group $Fd\bar{3}m$). Representative examples for the samples with various substitution levels are shown in Fig. 1(A and B).

Fig. 2 shows an example of the calculation of the unit cell parameter for C15T10M10N5 composition by the profile matching method in Fullprof software.

Some variations in the relative intensities of the peaks with the composition are attributed to the different nature of the substituting cations, which can reside in octahedral and/or tetrahedral sites, affecting the diffraction from corresponding atomic planes. Thus, the magnetite-based spinel structure is flexible to accommodate significant amounts of different transition metal cations, affecting the distribution of Fe^{2+} and high spin Fe^{3+} in octahedral positions, and causing structural effects revealed by the changes in lattice parameters (Table 1). These changes may depend on selective redox properties of different transition metal cations, as well as their distributions between tetrahedral and octahedral positions. The relative impact of different transition metal additives on the changes in unit cell parameter of $Fe_{2.8-x-y-z-p}Mg_{0.2}Cr_xTi_yMn_zNi_pO_4$ (Δa) was assessed by multivariant fitting of the data in Table 1, combined with additional results from a previous work,[14] yielding:

$$\Delta a \approx 0.00022 \quad 0.00298x + 0.00751y + 0.0113z \quad 0.00563p \quad (1)$$

where coefficients 0.00298, 0.00751, 0.01131 and 0.00563 give the dependence on contents of Cr, Ti, Mn and Ni, respectively. It should be noticed that the differences in lattice parameters are determined not only by the cation size, but also by its preference to reside in octahedral and/or tetrahedral sites of the spinel structure.[22] In addition, one should not exclude

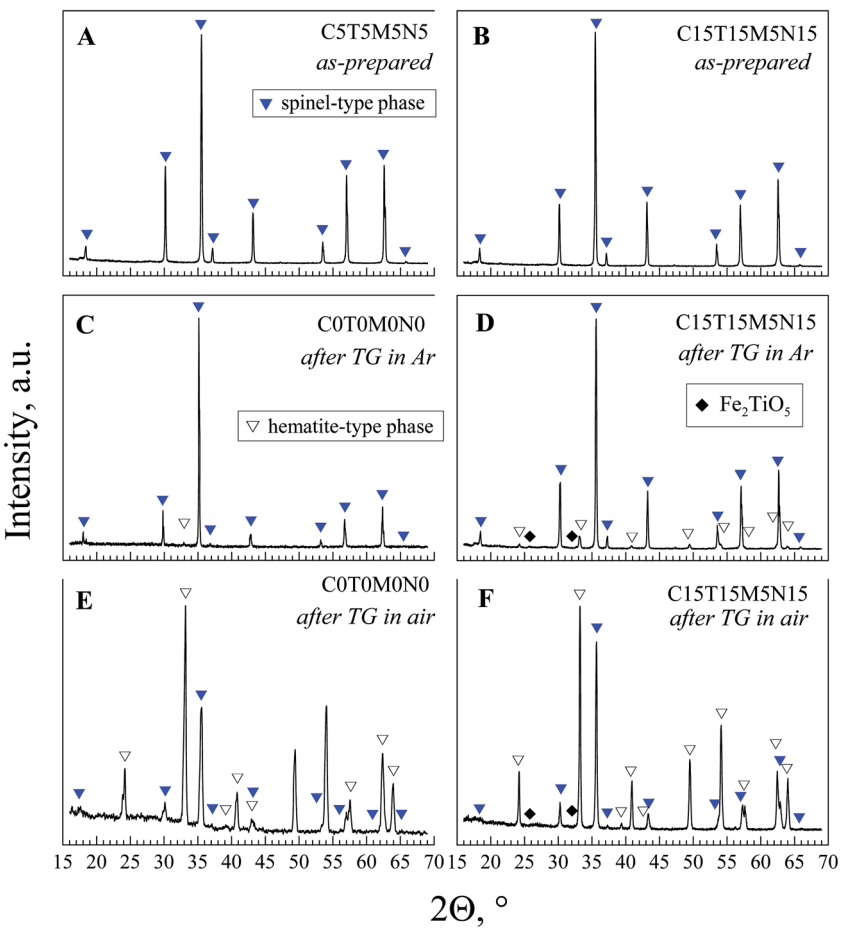

Fig. 1 Examples of XRD patterns for the as-prepared CTMN materials and corresponding samples after TG analysis in Ar and air atmospheres.

This journal is © The Royal Society of Chemistry 2016

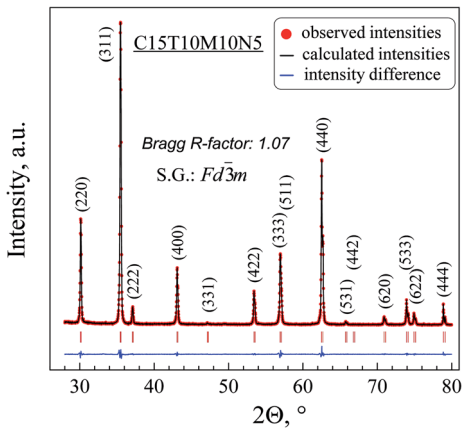

Fig. 2 Observed, calculated and difference XRD patterns for C15T10M10N5 multicomponent spinel.

possible contributions of other point defects such as cation vacancies or interstitial cations.[14] Chromium additions cause slight decrease in lattice parameter, as expected for preferential occupancy as Cr^{3+} in octahedral positions,[23] and by taking into account a slight difference between the ionic radius of Cr^{3+} ($\approx$0.061 nm) and high spin Fe^{3+} (0.0645 nm), as follows:

$$0.5xCr_2O_3 + (Fe_{1-\alpha}^{3+}Mg_{\alpha}^{2+})_{tet}(Fe_{1+\alpha}^{3+}Fe_{0.8}^{2+}Mg_{0.2-\alpha}^{2+})_{oct}O_4 \rightarrow (Fe_{1-\alpha}^{3+}Mg_{\alpha}^{2+})_{tet}(Fe_{1-x+\alpha}^{3+}Fe_{0.8}^{2+}Mg_{0.2-\alpha}^{2+}Cr_x^{3+})_{oct}O_4 + 0.5xFe_2O_3 \quad (2)$$

Note that Mg^{2+} is likely to occupy mainly octahedral sites (0.2 α) but still with a significant fraction (α) in tetrahedral sites.[24]

By analogy with reported information on the Fe_3O_4–Fe_2TiO_4 system[25] one expects tetravalent Ti^{4+} in octahedral positions. Thus, lattice expansion may result from differences between the average of relatively small radius of Ti^{4+} (0.0605 nm) and high spin Fe^{2+} (0.078), substituting high spin Fe^{3+} (0.0645 nm), as follows:

$$yTiO_2 + (Fe_{1-\alpha}^{3+}Mg_{\alpha}^{2+})_{tet}(Fe_{1+\alpha}^{3+}Fe_{0.8}^{2+}Mg_{0.2-\alpha}^{2+})_{oct}O_4 \rightarrow (Fe_{1-\alpha}^{3+}Mg_{\alpha}^{2+})_{tet}(Fe_{1+\alpha-2y}^{3+}Fe_{0.8+y}^{2+}Mg_{0.2-\alpha}^{2+}Ti_y^{4+})_{oct}O_4 + yFeO + 0.5yO_2 \quad (3)$$

Relevant literature on the Ni-containing spinels suggests preferential valence state Ni^{2+} and octahedral positions.[14,23,26] Presence of Ni^{3+} species in spinel lattice in Ar atmosphere at high temperatures is also unlikely, although they might be present at lower temperatures in other spinels (*e.g.* $NiCo_2O_4$), as evidenced by room-temperature XPS studies in other work.[27] Still, this may be due to a closer similarity between the thermodynamics of redox changes in NiO_x and CoO_x oxides. Thus, charge and site conservation imply partial substitution of Fe^{2+} by Ni^{2+} in octahedral sites, and lattice contraction is consistent with the difference between the ionic radius of Ni^{2+} (0.069 nm) and high spin Fe^{2+} (0.078 nm). Still, A-site occupancy is likely to be higher for Mg^{2+} than for Ni^{2+},[28,29] and one may also consider partial transfer of Mg^{2+} from octahedral positions (0.072 nm) to tetrahedral sites (0.057 nm), as follows:

$$pNiO + (Fe_{1-\alpha}^{3+}Mg_{\alpha}^{2+})_{tet}(Fe_{1+\alpha}^{3+}Fe_{0.8}^{2+}Mg_{0.2-\alpha}^{2+})_{oct}O_4 \rightarrow (Fe_{1-\alpha-\beta}^{3+}Mg_{\alpha+\beta}^{2+})_{tet}(Fe_{1+\alpha+\beta}^{3+}Fe_{0.8-p}^{2+} \times Mg_{0.2-\alpha-\beta}^{2+}Ni_p^{2+})_{oct}O_4 + pFeO \quad (4)$$

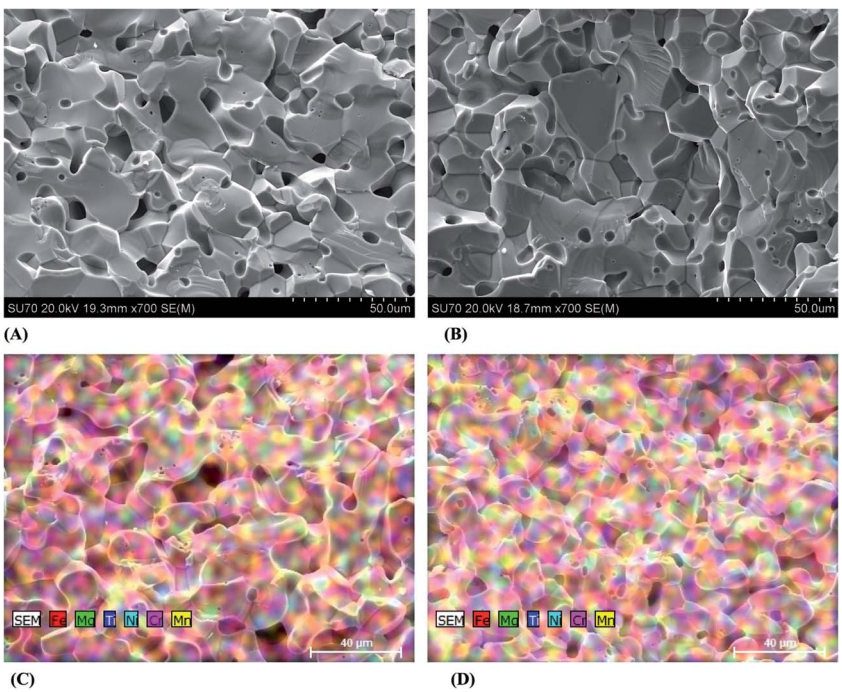

Fig. 3 Representative SEM micrographs (A and B) and EDS maps (C and D) for fractured C15T10M10N5 (A), C10T5M10N15 (B), C5T5M5N5 (C) and C10T15M15N5 (D) as-prepared samples.

Manganese shows a greater impact on the lattice parameter, and suggests preferential conditions for incorporation of Mn^{2+} in tetrahedral positions.[23,30] Its ionic radius (0.066 nm) is significantly higher than for Fe^{3+} in tetrahedral positions (0.049 nm). However, charge neutrality also implies decreasing concentration of Fe^{2+} cations with octahedral coordination, as predicted for:

$$zMnO + (Fe_{1-\alpha}{}^{3+}Mg_{\alpha}{}^{2+})_{tet}(Fe_{1+\alpha}{}^{3+}Fe_{0.8}{}^{2+}Mg_{0.2-\alpha}{}^{2+})_{oct}O_4 \rightarrow (Fe_{1-\alpha-z}{}^{3+}Mg_{\alpha}{}^{2+}Mn_{z}{}^{2+})_{tet}(Fe_{1+\alpha+z}{}^{3+}Fe_{0.8-z}{}^{2+}Mg_{0.2-\alpha}{}^{2+})_{oct}O_4 + zFeO \quad (5)$$

Thus, decreasing the fraction of high spin Fe^{2+} (0.078 nm) would imply a contribution to lattice shrinkage which would nearly cancel the difference between Mn^{2+} and Fe^{3+} in tetrahedral positions. In addition, one may also consider a distribution of Mn^{2+} in tetrahedral positions and Mn^{3+} in octahedral positions,[31,32] or even co-distributions of Mn^{2+} and Mn^{3+} in octahedral positions.[14] Thus, additions of Mn are likely to exert complex structural changes, with impact on properties.

Microstructural features of ceramic samples may also affect conductivity and other relevant properties, as well as redox kinetics, mainly when the actual firing conditions yield quite porous samples (Table 1). Still, the differences in relative density (Table 1) are rather minor. Secondly, the results of combined SEM/EDS studies did not reveal any noticeable differences in the grain size, pore geometry and pore size distributions, or presence of compositional inhomogeneities. Selected examples of SEM micrographs (Fig. 3A and B) and EDS maps (Fig. 3C and D) reflect the overall picture for all studied materials.

Electrical and redox properties are expected to depend on the oxidation states of the transition metal additives, combined with co-addition of Mg^{2+}, their preferential octahedral or tetrahedral coordination, overall effects on the $[Fe^{2+}]:[Fe^{3+}]$ ratio in octahedral positions, and capability to participate in electron hopping; this may also indirectly imply the crystallographic changes, for their effects on the carrier mobility. The general trends (Fig. 4) are similar to those observed for $(Fe,Mg,Al)_3O_4$ (ref. 9, 12, 13 and 22) and $Fe_{2.6}Me_{0.2}Mg_{0.2}O_4$ (Me = Ni, Cr, Ti)[14] spinels, attributed to the peculiarities of the defect chemistry mechanisms in spinels, including contributions of interstitial cation formation or cation vacancies at lower temperatures, and the onset of partial decomposition of the spinel phase.

Indeed, the results of TG analysis of powdered samples on heating in Ar confirm that the as-prepared CTMN ceramics are metastable at low temperatures (Fig. 5), in agreement with related literature.[9,12 14,22] The XRD analysis of the samples after TG studies in Ar (Fig. 1B and C) revealed a noticeable fraction of the hematite-type phase (Table 2). Thus, one may attribute a rapid conductivity drop, observed for several compositions at temperatures below 1280 K (Fig. 4), to the onset of secondary phases, suppressing the electronic charge transport.

The results on oxygen partial pressure dependence of the total conductivity (Fig. 6) also indicate the onset of phase decomposition on shifting from low $p(O_2)$ to more oxidizing

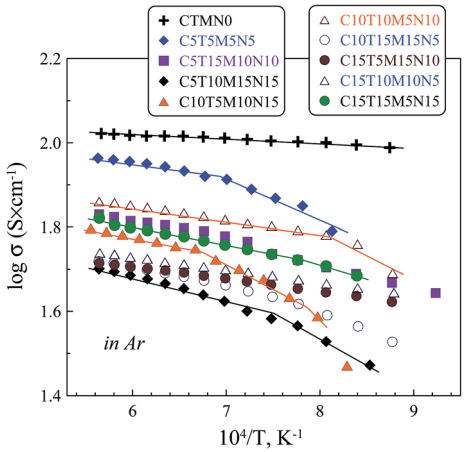

Fig. 4 Temperature dependence of the total conductivity of CTMN spinels, measured in Ar.

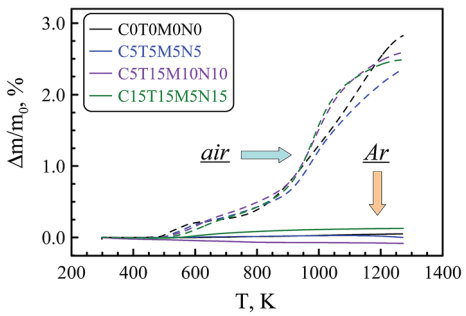

Fig. 5 Relative weight change of the powdered as-prepared CTMN spinel samples on heating in Ar (solid lines) and air (dashed lines).

conditions and decreasing temperature, accompanied with a sudden conductivity drop. Thus, one considered mainly high temperature conductivity data to analyse the impact of different transition metal additives. It should be noticed that below 1200 K all samples demonstrated slow equilibration kinetics on cooling and, correspondingly, a gradual conductivity drift with time.

The electronic transport in ferrospinels is mainly restricted to the octahedral sites and is expected to occur by small polaron mechanism, *via* hopping between Fe^{3+} and Fe^{2+} in octahedral sites.[33 36] In magnetite-based spinels the conductivity is roughly

Table 2 Phase composition of CTMN powders after TG analysis in Ar and air atmospheres, estimated from the XRD results

	After TG in Ar		After TG in air	
Composition	Spinel, % wt	Hematite, % wt	Spinel, % wt	Hematite, % wt
C0T0M0N0	~98	~2	0	100
C5T5M5N5	99	1	14 ± 4	86 ± 6
C5T15M10N10	93 ± 3	7 ± 1	18 ± 3	82 ± 6
C15T15M5N15	91 ± 5	8.7 ± 0.9	15 ± 4	85 ± 6

This journal is © The Royal Society of Chemistry 2016

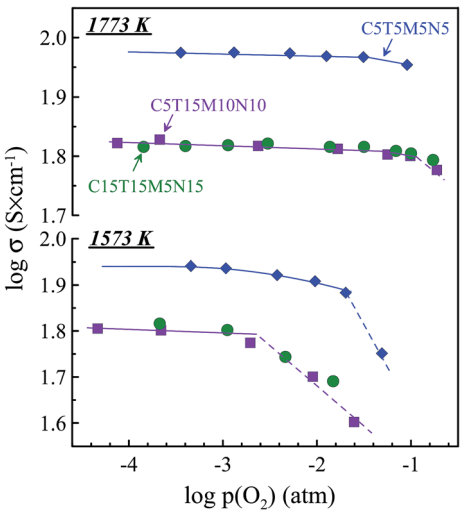

Fig. 6 Examples of the oxygen partial pressure dependence of the total conductivity for CTMN spinels at 1773 and 1573 K.

proportional to the probability of hopping, *i.e.* $[Fe^{2+}]_{oct}[Fe^{3+}]_{oct}$ concentration product in the octahedral positions.[9,14]

In the actual compositions, the effects exerted by the substitution are expected to be determined mainly by the changes in $[Fe^{2+}]$ fraction,[9,14] which, in turn, depends on the concentration and charge of the substituting cations (eqn (2)–(5)). Therefore, one assumed linear contributions of the concentration of each substituting cation to the total conductivity, as expected for generic charge neutrality conditions, as follows:

$$\frac{\sigma \quad \sigma_{C0T0M0N0}}{\sigma_{C0T0M0N0}} = a_{Cr}x + a_{Ti}y + a_{Mn}z + a_{Ni}p \qquad (6)$$

where a_{Cr}, a_{Ti}, a_{Mn}, a_{Ni} denote effects of corresponding additives on electrical conductivity relative to the non-substituted composition C0T0M0N0.

The analysis of composition effects was based on the Taguchi experimental planning (Table 1), combined with additional data for $Fe_{2.6}Me_{0.2}Mg_{0.2}O_4$ compositions (Me = Cr, Ti, Mn, Ni) from the ref. 14. By applying a multivariable least square method one obtained the parameters shown in Fig. 7, and the relative quality of fitting is illustrated in Fig. 8, by comparing

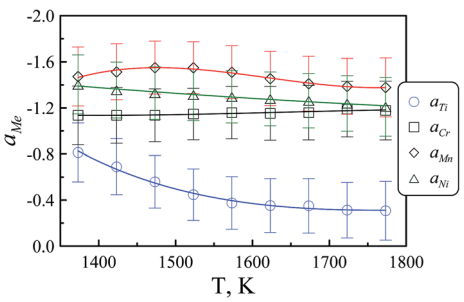

Fig. 7 Results on fitting the electrical conductivity data (Fig. 3 and ref. 14) using eqn (6): estimated impacts for each transition metal cation.

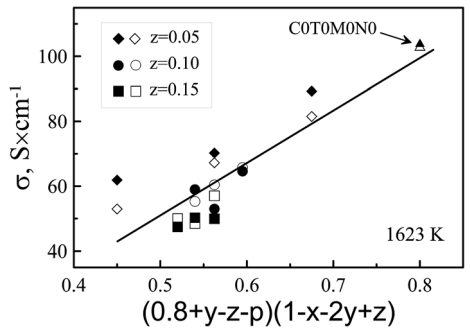

Fig. 8 Comparison of experimental conductivity data of $Fe_{2.8-x-y-z-p}Mg_{0.2}Cr_xTi_yMn_zNi_pO_4$ spinels at 1623 K (closed symbols) and corresponding model behaviour described by eqn (6) (open symbols). The symbols denote the relative contents of Mn. The solid line shows the linear trend for experimental data.

the experimental conductivity at a representative temperature (1623 K) and corresponding fitting.

These results are plotted *versus* $(0.8+y \quad z \quad p)(1 \quad x \quad 2y+z)$, which is a measure of the polaron probability factor in octahedral sites $[Fe^{2+}]_{oct}[Fe^{3+}]_{oct}$ (per formula unit), if one considers the expected charge and site changes described by eqn (2)–(5), also with prevailing Mg^{2+} in octahedral sites. Though Fig. 7 suggests negative impacts for every transition metal oxide, typically in the order Ti < Ni < Cr < Mn, differences between Cr, Mn and Ni are still within the error bar. In all cases the calculated impacts indicate that additions of different transition metal oxides affect hopping between Fe^{2+} and Fe^{3+} in octahedral sites, as emphasized in Fig. 8; this includes the additives effects (Ti^{4+}, Mn^{2+} and Ni^{2+}) on the fraction of Fe^{2+}, with expected octahedral coordination, and a competition between additives (mainly Mg^{2+}, Cr^{3+}, Ti^{4+} and Ni^{2+}) and $(Fe^{3+})_{oct}$ for the remaining octahedral sites.

Accordingly, one expects negative impact of the redox stable Cr^{3+} on $(Fe^{3+})_{oct}$, by completion for octahedral sites, and a negative impact of acceptor type Ni^{2+} on $(Fe^{2+})_{oct}$. The overall effect of donor type Ti^{4+} combines a positive role on $(Fe^{2+})_{oct}$ and the negative effect on $(Fe^{3+})_{oct}$, this is consistent with a relatively low impact on conductivity (Fig. 7).

The prevailing effects of manganese additions on charge and site occupancy (Eq.(5)) predict a combination of negative impact on $(Fe^{2+})_{oct}$ and positive impact on $(Fe^{3+})_{oct}$; this is not consistent with its worse overall effect on conductivity, and indicates presence of more complex effects. For example, one cannot exclude more complex equilibria between redox pairs (*e.g.* $Mn^{2+} + Fe^{3+} \leftrightarrow Mn^{3+} + Fe^{2+}$),[28] with strong preference of Mn^{3+} cations to reside in octahedral sites, while Mn^{2+} is expected to have higher affinity for tetrahedral sites.[14] Strongest structural effects of Mn are also likely to affect the mobility of polarons, as revealed by the analysis of correlation factors for combined effects of Mn with other additives (Table 3).

For example, one finds stronger correlation for interactions between additions of Cr and Mn (*i.e.*, *xz*) than for interactions of Cr with other additives Ti (*xy*) or Ni (*xp*). Similar conclusions are revealed by higher correlation factors for interactions between

Table 3 Pearson's correlation factors for combined effects of different additive pairs on the conductivity of $Fe_{2\,8\,x\,y\,z\,p}$-$Mg_{0\,2}Cr_xTi_yMn_zNi_pO_4$ spinels at 1623 K

Correlation factors at 1623 K							
	r		r		r		r
x^2	0.54	yx	0.56	zx	0.76	px	0.50
xy	0.75	y^2	0.57	zy	0.73	py	0.51
xz	0.90	yz	0.73	z^2	0.78	pz	0.72
xp	0.69	yp	0.51	zp	0.72	p^2	0.47

Ti and Mn (yz) and between Ni and Mn (pz). This is also confirmed by the results presented in Fig. 8, where stronger negative deviations from the main trend line also correspond to the samples with highest contents of Mn ($z = 0.15$) and positive deviations are observed for the lowest Mn contents ($x = 0.05$). Interactions between additions of Mn and other additives may be understood by taking into account that conductivity by polaron hopping ($\sigma \propto P\mu$) depends both on hopping probability $P = [Fe^{2+}]_{oct}[Fe^{3+}]_{oct}$, determined by a combination of different additives, and mobility (μ), affected by structural effects of Mn cations. Still, more detailed redox and structural studies, including XPS, possibly combined with Seebeck coefficient[37] measurements and lattice simulations, are needed to elucidate possible role of manganese species in electronic transport and relevant effects on the oxidation state of iron cations. Some clues may be obviously linked to the redox activity of manganese cations, as Mn^{2+} and Mn^{3+} are expected to have different preferred coordination, they may act as a buffer, forcing other cations to occupy rather unusual lattice sites, with dynamic and hardly predictable effects on the electronic transport, which are also dependent on the redox conditions.

The impact coefficient a_{Ti} also shows a noticeable temperature dependence, being less negative in the high temperature range. Though partial reduction to Ti^{3+} may occur at very high temperatures, in neutral Ar atmosphere, the Ti^{3+}/Ti^{4+} redox couples are unlikely to play a significant role in the electronic transport, as the concentration of titanium in studied spinels remains at least 15 times lower than corresponding minimal total concentration of iron. Thus, this is unlikely to explain the observed decrease in absolute of a_{Ti} (greater than 2 times from 1773 to 1373 K). A more plausible explanation may be based on the lower redox stability of Ti-rich ferrospinels,[14] resulting in partial phase decomposition and corresponding decrease in the total conductivity at lower temperatures.

Though no signs of phase decomposition were found for all studied materials at temperatures above 1500 K, the onset of phase decomposition is usually revealed by abnormal changes in electrical conductivity at temperatures below about 1373 K (Fig. 4). This is also confirmed by oxygen uptake at temperatures above 500 K on heating even in Ar atmosphere ($p(O_2) \sim 10^{-5}$ atm) (Fig. 5), resulting in separation of hematite-type and Fe_2TiO_5 phases (Fig. 1C and D). However, it appears difficult to quantify the effects of composition of the multicomponent spinels on redox properties and phase stability. In particular, assessment of $p(O_2)$, T – stability limits requires long-time equilibration and remains somewhat uncertain, due to sluggish redox-induced phase decomposition of the ferrospinels,[12] especially at relatively low temperatures. Phase decomposition only tends to become massive on heating in air, with hematite presented as a major phase (Fig. 1E and F; Table 2). It is important to notice that the only secondary phases detected by XRD after oxidative decomposition were hematite and/or Fe_2TiO_5, without any evidence of other transition metal oxides. A plausible explanation may include partial substitution in hematite by minor amounts of Cr and Mn, formation of spinel-type $NiFe_2O_4$ and $CrFe_2O_4$, overlapping XRD peaks of the main spinel phase, or its partial enrichment with the transition metal cations. This also complicates the comparative analysis of impacts of different transition metal additives on the redox stability. However, some guidelines can be proposed based on the TG curves taken in air and quantification of the phase composition after TG analysis. The compositions, containing more transition metal additives, appear to be less redox stable, resulting in higher oxygen uptake (Fig. 5) at 950–1150 K and larger amount of hematite impurity (Table 2). Assuming that the major part of the relative weight increase (Fig. 5) is provided by Fe^{2+} oxidation, these cations are more susceptible to oxidation in multicomponent ferrospinels. Otherwise one should observe an increase of oxygen uptake in the order C15T15M5N15 < C5T15M10N10 < C5T5M5N5 < C0T0M0N0, which corresponds to the increase of the total iron concentration in the samples. It is noteworthy that extrapolation of the TG curves, obtained in air (Fig. 5), to the temperatures above 1300–1350 K, where the oxidation is more rapid and massive, gives the above sequence for the expected oxygen uptake. In the intermediate temperature range (950–1150 K) the redox tolerance is mostly determined by the distribution of Fe^{2+} cations between tetrahedral and octahedral sites,[38] interdiffusion of the constituting cations and cation vacancies[39] and thermodynamic stability of the possible reaction products compared to the main spinel phase. Thus, for more complex chemical composition one may expect more favourable pathways for the oxidation reaction to occur. The results on the oxygen partial pressure dependence of the total conductivity (Fig. 6) also confirm this conclusion. The conductivity of slightly-substituted C5T5M5N5 composition starts to drop at higher oxygen partial pressures compared to the samples, containing more transition metal additives, indicating higher tolerance against oxidation. Hence, multicomponent spinels, containing various redox-active cations, may be more prone to the oxidative decomposition, imposing corresponding limitations on their application at relevant intermediate temperatures in oxidizing conditions.

A decrease of the electrical conductivity due to the redox-promoted effects in multicomponent ferrospinels is not the only factor, which may impede potential applications at high temperatures. Thermochemical expansion of the spinel ceramics may be also greatly affected by the redox processes, as illustrated by Fig. 9.

It should be noticed that the thermal expansion behaviour of the ferrospinels in quasi-inert atmospheres itself is quite complex and depends on the changes in concentration of point

 This journal is © The Royal Society of Chemistry 2016

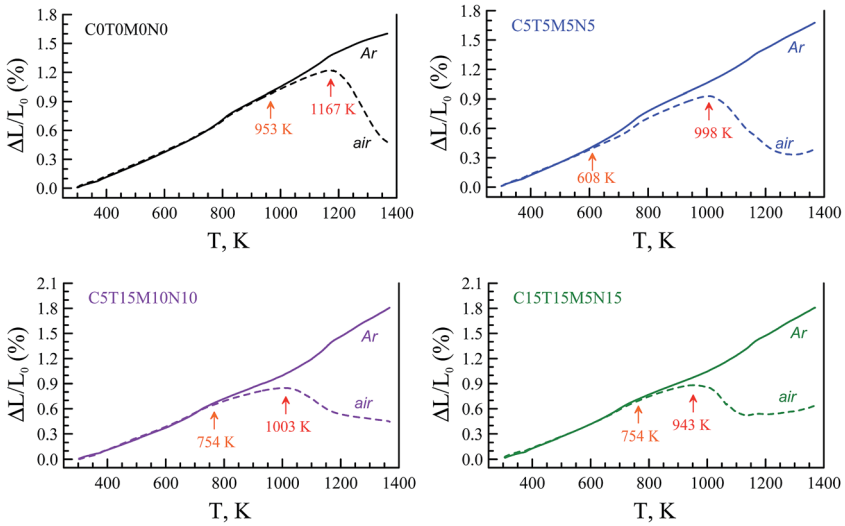

Fig. 9 Dilatometric curves for several representative CTMN spinels in Ar and air on heating. The arrows show the regions where various oxidative decomposition reactions occur.

defects and/or their rearrangements in tetrahedral and octahedral sublattices.[9,12 14,40] Corresponding thermal expansion coefficients (TECs), calculated for the temperature ranges where linear trends for relative length change were observed, are listed in the Table 4. At low (~373–723 K) and high (~1123–1373 K) temperatures in Ar atmosphere the TEC's of the studied materials lie within the range of (13.5–14.6) × 10^{-6} K^{-1} and (11.1–21.6) × 10^{-6} K^{-1}, correspondingly, showing a tendency to increase with the substitution level.

Similar thermal expansion in low temperature range was also observed in air atmosphere. Further heating in air results in noticeable volume changes and even contraction of the ceramics, which can be attributed to the oxidation of Fe^{2+} cation to smaller Fe^{3+} and massive formation of the hematite-type phases. The onset of redox-induced deviations in expansion behaviour for base C0T0M0N0 composition occurs at higher temperature (~953 K) compared to the multicomponent samples, again suggesting that the redox stability decreases on substituting with multiple transition metals. However, a simple comparison of the conditions, which correspond to ceramics collapse on the dilatometric curves, may not be enough to understand the impact of the chemical composition on redox tolerance and corresponding thermochemical behaviour. In particular, those sudden dimensional changes might also depend on the presence of random microscopic defects in ceramic samples, which further readily evolve on oxidation. Assuming that the oxidation process starts at the ceramics surface, the obtained results point out that for high-temperature practical applications, requiring sufficiently conductive and mechanically stable bulk ferrospinels, the thermocycling should be performed relatively fast in the temperature range of 1000–1400 K, where the oxidation may be fairly detrimental for the performance.

Table 4 Thermal expansion coefficients of CTMN spinels

	Average thermal expansion coefficients		
Composition	$p(O_2)$, atm	T, K	$(\bar{\alpha} \times 106) \pm 0.1$, K ^{1}
C0T0M0N0	10 ^{5}	373 723	13.5
		773 1073	17.2
		1198 1373	11.1
	0.21	373 723	13.3
		773 1123	14.8
C5T5M5N5	10 ^{5}	373 623	13.7
		723 1073	15.0
		1123 1373	16.3
	0.21	373 773	13.5
		823 1023	9.6
C5T15M10N10	10 ^{5}	373 573	14.9
		723 973	14.0
		1123 1373	21.6
	0.21	373 773	14.6
C15T15M5N15	10 ^{5}	373 673	14.9
		723 1073	14.5
		1123 1373	20.3
	0.21	373 773	15.3

4. Conclusions

Single-phase multicomponent ferrospinels, derived from $Fe_{2.8}Mg_{0.2}O_4$ composition, co-substituted with transition metal cations (Cr, Ti, Mn, Ni), were prepared by solid state route, followed by sintering at 1773 K for 10 h in Ar. Relevant structural, microstructural, transport, thermal and redox properties were assessed by combined XRD/SEM/EDS, thermal gravimetry, dilatometry and electrical conductivity studies at various temperatures and oxygen partial pressures. Multiple substitutions with transition metal cations were found to decrease the electrical conductivity, with comparable impacts observed for chromium and nickel additions. The negative impact of manganese additions on electrical conductivity is more complex and implies interactions with other additives in multicomponent spinels, probably indicating

negative impact on mobility. The presence of higher amount of titanium was proved to be favorable to retain higher electrical conductivity, by promoting the formation of Fe^{2+} cations and increased hopping probability. The redox stability of multicomponent spinels was poorer than for the base $Fe_{2.8}Mg_{0.2}O_4$ composition, imposing certain limitations on high-temperature applications. The most severe dimensional changes, induced by the redox processes in air, occur at 1000–1400 K and may result in a collapse of the corresponding ceramics.

Acknowledgements

Research leading to these results has received support from the European Union's Research Fund for Coal and Steel (RFCS) research program, under grant agreement IERO-RSF-PR-09099. This work was developed within the scope of the project CICECO-Aveiro Institute of Materials, POCI-01-0145-FEDER-007679 (FCT Ref. UID/CTM/50011/2013) and i3N institute with UID/CTM/50025/2013 project, financed by national funds through the FCT/MEC and when appropriate co-financed by FEDER under the PT2020 Partnership Agreement. The support from FCT, Portugal (grant IF/00302/2012) is also acknowledged. M. C. Ferro acknowledges support from RNME – Pole University of Aveiro and FCT project REDE/1509/RME/2005.

References

1 A. J. Moulson and J. M. Herbert, *Electroceramics: Materials, Properties, Applications*, 2003.
2 P. N. L. Lens, J. Virkutyte, V. Jegatheesan, K. Seung-Hyun and S. Al-Abed, *Nanotechnology for Water and Wastewater Treatment*, IWA Publishing, London, 2013.
3 A. S. Teja and P.-Y. Koh, *Prog. Cryst. Growth Charact. Mater.*, 2009, **55**, 22–45.
4 G. S. Parkinson, U. Diebold, J. Tang and L. Malkinski, in *Advanced Magnetic Materials*, ed. L. Malkinski, InTech, 2012.
5 *Handbook of Battery Materials*, ed. C. Daniel and J. O. Besenhard, Wiley-VCH Verlag GmbH & Co. KGaA, Weinheim, Germany, 2011.
6 E. Manova, T. Tsoncheva, C. Estournès, D. Paneva, K. Tenchev, I. Mitov and L. Petrov, *Appl. Catal., A*, 2006, **300**, 170–180.
7 S. Nie, E. Starodub, M. Monti, D. A. Siegel, L. Vergara, F. El Gabaly, N. C. Bartelt, J. de la Figuera and K. F. McCarty, *J. Am. Chem. Soc.*, 2013, **135**, 10091–10098.
8 R. J. Harrison and A. Putnis, *Am. Mineral.*, 1996, **81**, 375–384.
9 A. V. Kovalevsky, A. A. Yaremchenko, E. N. Naumovich, N. M. Ferreira, S. M. Mikhalev, F. M. Costa and J. R. Frade, *J. Eur. Ceram. Soc.*, 2013, **33**, 2751–2760.
10 D. R. Sadoway, *J. Mater. Res.*, 1995, **10**, 487–492.
11 H. Kim, J. Paramore, A. Allanore and D. R. Sadoway, *J. Electrochem. Soc.*, 2011, **158**, E101.
12 A. V. Kovalevsky, E. N. Naumovich, A. A. Yaremchenko and J. R. Frade, *J. Eur. Ceram. Soc.*, 2012, **32**, 3255–3263.
13 A. A. Yaremchenko, A. V. Kovalevsky, E. N. Naumovich, V. V. Kharton and J. R. Frade, *Solid State Ionics*, 2011, **192**, 252–258.
14 N. M. Ferreira, A. V. Kovalevsky, E. N. Naumovich, A. A. Yaremchenko, K. V. Zakharchuk, F. M. Costa and J. R. Frade, *J. Eur. Ceram. Soc.*, 2014, **34**, 2339–2350.
15 R. Liang, R. Tian, Z. Liu, D. Yan and M. Wei, *Chem.–Asian J.*, 2014, **9**, 1161–1167.
16 M. M. Mallapur and B. K. Chougule, *Mater. Lett.*, 2010, **64**, 231–234.
17 M. H. Zahir, K. Alhooshani, M. A. Jafar Mazumder and T. Suzuki, *Kinet. Catal.*, 2013, **54**, 578–585.
18 S. Rajakumar, R. Thirunakaran, A. Sivashanmugam, J. Yamaki and S. Gopukumar, *J. Electrochem. Soc.*, 2009, **156**, A246.
19 N. M. Ferreira, A. V. Kovalevsky, S. M. Mikhalev, F. M. Costa and J. R. Frade, *Phys. Chem. Chem. Phys.*, 2015, **17**, 9313–9325.
20 L. N. Harris, *Qual. Reliab. Eng. Int.*, 1989, **5**, 249.
21 J. Rodríguez-Carvajal, *Phys. B*, 1993, **192**, 55–69.
22 R. J. Hill, J. R. Craig and G. V. Gibbs, *Phys. Chem. Miner.*, 1979, **4**, 317–339.
23 X. Liang, Y. Zhong, S. Zhu, H. He, P. Yuan, J. Zhu and Z. Jiang, *Solid State Sci.*, 2013, **15**, 115–122.
24 F. Nakagomi, S. W. da Silva, V. K. Garg, A. C. Oliveira, P. C. Morais and A. Franco, *J. Solid State Chem.*, 2009, **182**, 2423–2429.
25 C. I. Pearce, C. M. B. Henderson, N. D. Telling, R. A. D. Pattrick, J. M. Charnock, V. S. Coker, E. Arenholz, F. Tuna and G. van der Laan, *Am. Mineral.*, 2010, **95**, 425–439.
26 N. Ponpandian, P. Balaya and A. Narayanasamy, *J. Phys.: Condens. Matter*, 2002, **14**, 3221–3237.
27 J. F. Marco, J. R. Gancedo, M. Gracia, J. L. Gautier, E. I. Ríos, H. M. Palmer, C. Greaves and F. J. Berry, *J. Mater. Chem.*, 2001, **11**, 3087–3093.
28 C. M. B. Henderson, J. M. Charnock and D. A. Plant, *J. Phys.: Condens. Matter*, 2007, **19**, 076214.
29 M. Airimioaei, M.-N. Palamaru, A. R. Iordan, P. Berthet, C. Decorse, L. Curecheriu and L. Mitoseriu, *J. Am. Ceram. Soc.*, 2014, **97**, 519–526.
30 V. M. Khot, A. B. Salunkhe, M. R. Phadatare, N. D. Thorat and S. H. Pawar, *J. Phys. D: Appl. Phys.*, 2013, **46**, 055303.
31 M. A. Denecke, W. Gunßer, G. Buxbaum and P. Kuske, *Mater. Res. Bull.*, 1992, **27**, 507–514.
32 K. Vamvakidis, M. Katsikini, D. Sakellari, E. C. Paloura, O. Kalogirou and C. Dendrinou-Samara, *Dalton Trans.*, 2014, **43**, 12754.
33 G. Maris, O. Shklyarevskii, L. Jdira, J. G. H. Hermsen and S. Speller, *Surf. Sci.*, 2006, **600**, 5084–5091.
34 T. O. Mason and H. K. Bowen, *J. Am. Ceram. Soc.*, 1981, **64**, 237–242.
35 J. Nell and B. J. Wood, *Am. Mineral.*, 1991, **76**, 405–426.
36 J. Nell, B. J. Wood and T. O. Mason, *Am. Mineral.*, 1989, **74**, 339–351.
37 F. K. Lotgering, *J. Phys. Chem. Solids*, 1964, 95–103.
38 B. Gillot, F. Jemmali, F. Chassagneux, C. Salvaing and A. Rousset, *J. Solid State Chem.*, 1982, **45**, 317–323.
39 R. Freer, *Mineral. Mag.*, 1980, **43**, 889–899.
40 D. Levy, G. Artioli and M. Dapiaggi, *J. Solid State Chem.*, 2004, **177**, 1713–1716.

 This journal is © The Royal Society of Chemistry 2016